A Large-Scale Three-Dimensional Imaging System Based On Laser Speckle

by

Michael Stephen Mermelstein

Submitted to the Department of Electrical Engineering and Computer Science
in partial fulfillment of the requirements for the degree of

Master of Science in Electrical Engineering and Computer Science

at the

MASSACHUSETTS INSTITUTE OF TECHNOLOGY

May 1995

Author .....
Department of Electrical Engineering and Computer Science
May 12, 1995

Certified by .....
Lyle G. Shirley
Lincoln Laboratory Research Staff
Thesis Supervisor

Certified by .....
Thomas F. Knight Jr.
Principal Research Scientist
Thesis Supervisor

Accepted by .....
Frederic R. Morgenthaler
Chairman, Departmental Committee on Graduate Students

A Large-Scale Three-Dimensional Imaging System Based On Laser Speckle

by

Michael Stephen Mermelstein

Submitted to the Department of Electrical Engineering and Computer Science
on May 12, 1995, in partial fulfillment of the
requirements for the degree of
Master of Science in Electrical Engineering and Computer Science

Abstract

In this thesis, I designed and implemented a three-dimensional scanner which is high-speed, noncontact, and scalable. The scanner measures optical interference (speckle) from a variable frequency laser to precisely determine the three-dimensional surface contour of a target object. The design consists of optical, electronic, and mechanical hardware as well as computer software. A prototype scanner was constructed and characterized. The instrument can measure an array of 256×256 surface heights to a resolution of 15 μm, and it can complete such a measurement along with the related computation in less than one minute. The design is discussed and representative data are presented. Finally, I demonstrate the feasibility of and suggest a few motivating applications for 3-D video.

Thesis Supervisor: Lyle G. Shirley
Title: Lincoln Laboratory Research Staff

Thesis Supervisor: Thomas F. Knight Jr.
Title: Principal Research Scientist

Acknowledgments

Sincere thanks to my supervisors, past and present, and to my family for their encouragement.

Thanks also to the members of the Lincoln Laboratory Group 35 Laser Speckle Laboratory for their generous assistance. In particular, I thank Emory Ariel for helping with the mechanical aspects of the laser, Gregory Hallerman for his vital guidance with the optics of various incarnations of my thesis, Harold Payson, the proponent of the image-plane speckle 3D scanner, for sharing his ideas, and Lyle Shirley for his insightful counsel and also for seeing that the Speckle Lab stays a flexible and enjoyable research environment.

From the Artificial Intelligence Laboratory, I thank André DeHon for contributing his SBus I/O card and timely assistance with the Allegro CAD system, and finally, Tom Knight for his open collection of resources and his general good advice.

This work was supported by the U.S. Army Space and Strategic Defense Command, the Lincoln Laboratory Advanced Concepts Committee, and the Lincoln Laboratory Civil Sector Team.

Contents

List of Figures

Chapter 1

Introduction

Application to real-world problems has been a dominant theme throughout the history of computers. A principal obstacle to that application has often been in getting information from the real world into the world of a computer's memory. The remote-sensing 3D scanner discussed herein is a tool to overcome that obstacle in a large number of applications.

1.1 Historical context

In the last thirty years, computer graphics devices have evolved from vector displays only capable of line-drawing, to high-resolution color pixelized displays such as a typical workstation CRT. Currently, we are witness to the emergence of various 3D output technologies such as stereoscopic head-mounted displays and aluminum dust 3D printing devices. Likewise, during the same period of time, input devices have evolved from punchcards and ribbons to keyboards to the now-commonplace mouse, microphone, and video camera—echoing the trend toward higher dimensions and higher input rates.

Several 3D input devices already exist and have gained acceptance in a number of fields. The most successful of those devices are mentioned below.

1.2 Current 3D input devices

1.2.1 Coordinate Measuring Machines

Coordinate Measuring Machines (CMM's) have long been the preferred method of acquiring surface contours of machined and sheet-metal parts in industry.

A CMM generally consists of a stage where the part to be measured can be mounted securely. A robotic arm touches the part with a stylus tip which is usually outfitted with an electronic depth-gauge. Data from motor encoders combined with depth-gauge readings from the stylus comprise the information about the location of the part's surface. Software directs the arm to touch down on the part in some matrix of points in order to attain a complete surface map. A representative CMM can measure 40 points per minute within a target volume of roughly $50 \times 50 \times 50$ cm with a resolution of 10 μm [6].

The CMM is a somewhat robust instrument for general-purpose metrology but has some notable limitations. First and foremost is the set of parts that can *not* be measured by a CMM. Such parts are either too large for the largest reasonable CMM, or too complex geometrically to be measured by this strategy. As a result, airplane wings and fuselage panels as well as many complex gears, for example, pose a challenge to CMM manufacturers.

1.2.2 Optical Triangulation Techniques

Plastic surgeons often want to measure the surface contour of some part of a patient's body—the face, for example. But poking a patient tens of thousands of times in the face over a several-hour period would eventually diminish a doctor's client base. So plastic surgeons generally turn to a non-contact scanning technique rather than to CMM-type technologies.

The scanner technology most commonly used by plastic surgeons is that of triangulation. See Figure 1-1. In this technique, a beam of light (typically a collimated laser beam) illuminates a spot on the object to be measured. The spot is detected by

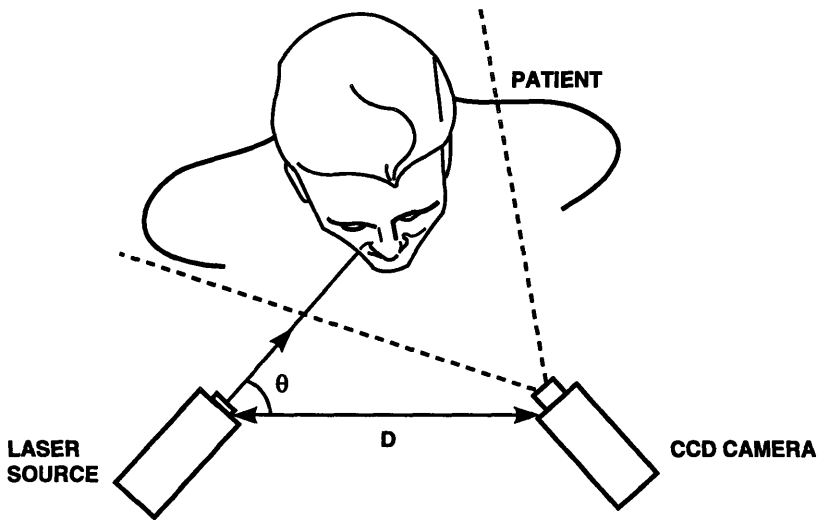

Figure 1-1: Typical triangulation setup.

a camera which is mounted at a known orientation with respect to the laser source. From the array coordinates of the bright cluster of pixels in the camera's field of view, the range of the target from the laser can be inferred. Generally, the beam is directed up and down tracing out a line from, in my example, the neck to the forehead while the whole apparatus is either translated by the face or moved all the way around the head to acquire a complete surface contour. The most popular of these scanners are made by a company named Cyberware.

Triangulation techniques have several advantages. A noncontact scanner is often preferable to a metal probe as it is in my example as well as for a range of soft materials commonly scanned today, such as clay models used by designers and computer animators. The scan times are far shorter because the robotics does not have to change directions for each measurement point. A spinning polygonal mirror can rapidly scan vertically while a slower drive motor can perform the translation or rotation of the source-detector assemblage. These scanners can offer 50 μm resolution in a time-frame of one to fifteen minutes for a scan of around 500 $\times$ 500 points [5].

As with CMM's, triangulation fails in a number of cases. A surface detail such as a well or a tower might keep the source beam from some part of the surface, i.e. the bottom of the well or the far side of the tower. Furthermore, it hasn't been reasonable (as yet) to apply this technology to objects larger than several feet across; thus, triangulation yields to a size limitation just as CMM's do.

1.2.3 Medical volumetric imaging techniques

There are now several medical scanners which can provide three-dimensional information about a sample placed in the machine. Unlike the scanners discussed above, techniques such as magnetic resonance imaging (MRI) and computer aided (X-ray) tomography (CAT) can resolve structures within the volume of a target sample.

These technologies are often allergic to certain materials (such as metal) and without exception involve placing the sample in a machine that scales poorly (in size and cost) with the size of the sample chamber.

1.2.4 Interferometric microscopes, defocus techniques, and others

Finally, there are a number of scanners that are based on principles that only can be applied within reason to small objects. These, along with the medical volumetric scanners mentioned above have their dedicated niches and are not "general-purpose" enough to spend time with a detailed comparison. I mention them only as a gesture to completeness.

1.3 Where laser speckle fits in

The Laser Speckle Laboratory, part of MIT Lincoln Laboratory's Signature Studies and Analysis Group, has been investigating the information content of speckle under the direction of Lyle Shirley since 1990. The lab has developed several innovative remote sensors based on this information content including remote-surface angle-sensors

and free-body projected-spin-axis detectors, as well as a number of 3D scanners.

Novel schemes based on the wavelength dependence of laser speckle can combine low-cost, high speed, and high resolution with non-contact measurement and scalability (the potential to measure objects of a wide range of sizes with the same, small instrument). In contrast, among the non-speckle 3D input schemes currently used, there exist intrinsic tradeoffs between resolution, scan speed, target size, and cost of the scanner.

Applications of a high-speed, low-cost, non-contact, remote-sensing, scalable 3D input device abound in the entertainment, military, and manufacturing industries. These are the applications which will nurture the technology and deliver it to our desktops.

Chapter 2

Apparatus

A 3D scanner based on laser speckle sets up an interference pattern by combining coherent light from at least two beam paths. The Laser Speckle Laboratory has experimented with many optical configurations to acquire 3D data. The technique implemented here (suggested by Harold Payson of the Speckle Lab) involves the scanner flood-illuminating a surface to be measured as well as a flat surface (a reference plate) with coherent light. The wavelength dependence of the interference patterns generated by the pair of surfaces contains 3D information [7].

The apparatus proper is made up of three parts: the laser source, some optics, and a detector.

2.1 Tunable coherent source

2.1.1 Laser specifications

The range resolution of a speckle measurement is essentially determined by the tuning bandwidth of the laser source. An external cavity diode laser with about a 15 THz tuning range was found, providing a raw range resolution of 10 μm. This laser is made by Nu Focus.

The laser head is quite small: about $9 \times 9 \times 13$ centimeters. It is also rugged and portable (unlike typical tunable lasers). Figure 2-1 is a photograph of the laser head.

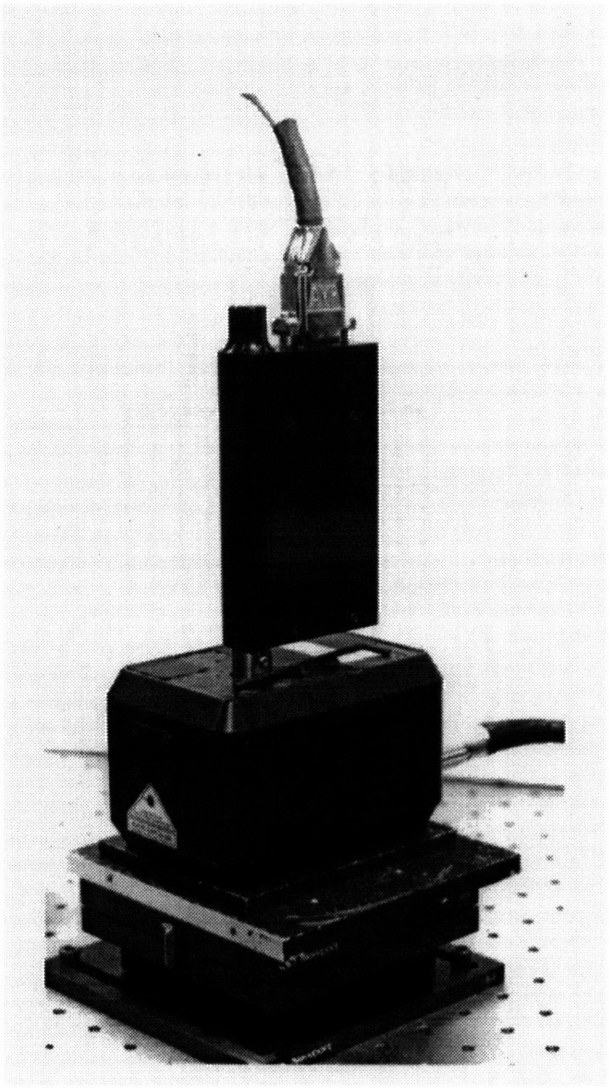

Figure 2-1: Photograph of the external cavity diode laser head coupled with the new motor drive.

The diode generates 5 to 10 mW in the range of 769 to 791 nm. Depending on the surface coating of the target, this is enough power to sufficiently illuminate one hundred to two hundred square centimeters of surface area.

2.1.2 Superior cavity design

Previous tunable laser designs, including the Ti:Sapphire ring laser (shown in Figure 2-2) used for the Speckle Laboratory's pioneering work in speckle-based 3D imaging, all use a number of servo-actuators to change the laser frequency and maintain a lasing condition. These designs require a settling time between frequency steps that depends on an electro-mechanical feedback system of impressive complexity. Nu Focus's laser cavity was designed so that a single motion scans the effective cavity length while simultaneously preserving the conditions (to a part in a thousand) for laser resonance. See Nu Focus's patent [1] for a detailed description of how this was accomplished.

2.1.3 Linear actuator

The "picomotor" supplied with the laser to control this single motion was slow and did not repeatably translate the same amount for the same input as a normal stepper should. It also produced an intolerable whining sound when enabled. Therefore, the picomotor was replaced (after some structural modification to the laser) by a more repeatable, limber, and quiet motor: a Newport PM-5000 linear driver. The motor's job is to set the effective cavity size by moving a mirror mounted on a swing-arm. See Figure 2-3. The PM-5000 is capable of tuning the laser over its entire tuning range in well under a tenth of a second as well as of accurately scanning twenty-five thousand times slower.

Outfitted with a new motor, and interfaced to a host computer, the Nu Focus laser is well suited for high-speed 3D scanning applications.

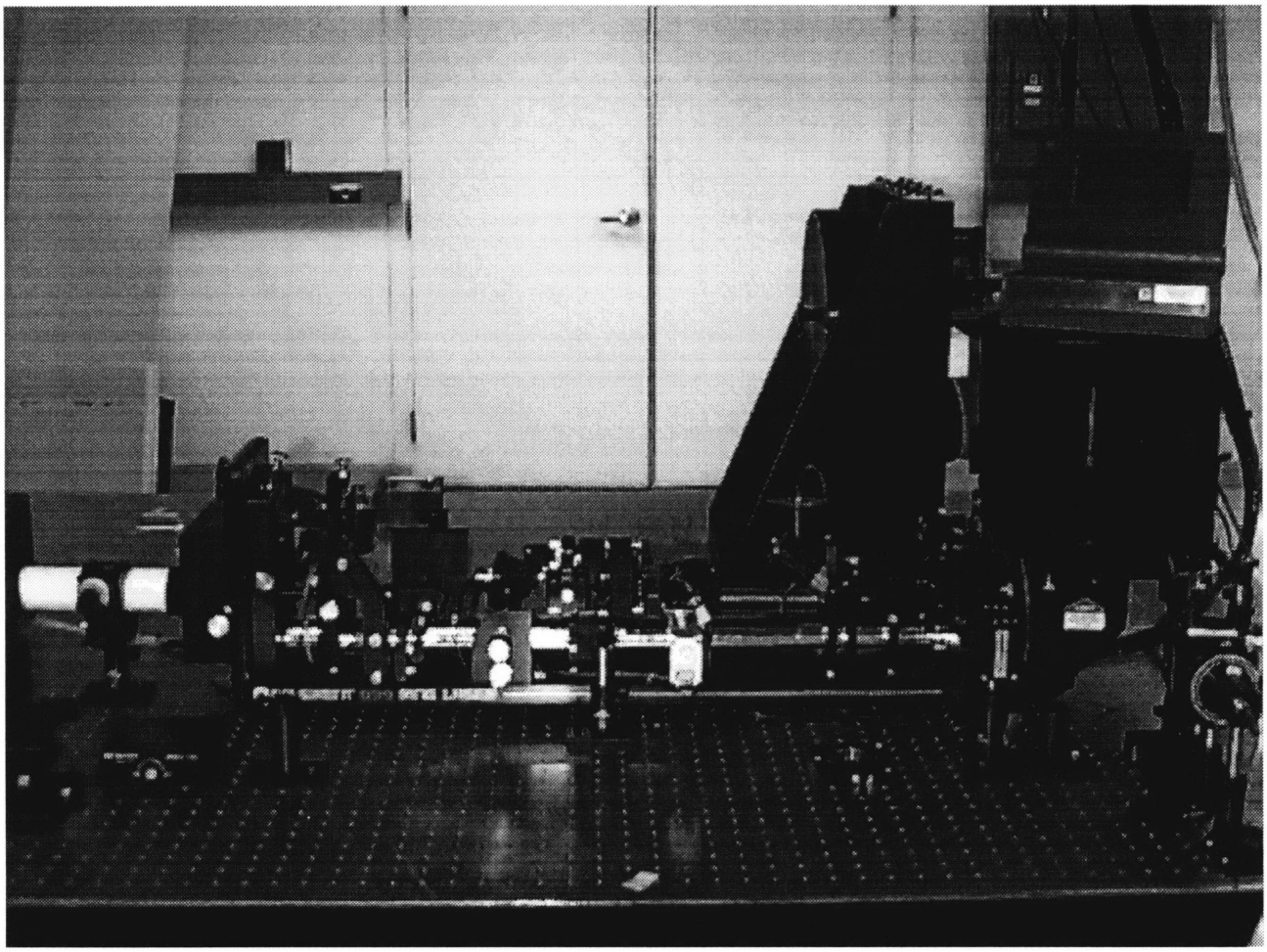

Figure 2-2: Ti:Sapphire ring laser with its complicated cavity design and numerous servos.

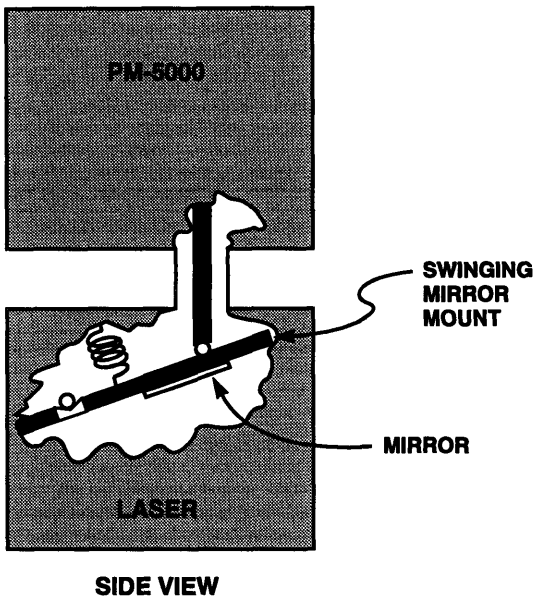

Figure 2-3: Schematic diagram showing how the PM-5000 linear actuator sets the position of a cavity mirror in the laser head.

2.2 Optical System

A typical 3D speckle scanning setup combines light reflecting from a known "reference" object (often a point or a plane) with light from the unknown surface. The specific configuration for the optics hinges on the method chosen for creating a reference optical path. Figure 2-4 illustrates the setup used. Because the interference at the target's surface is measured, this setup is said to use "image-plane" detection. The setup was chosen for its simplicity and because it uses diverging light. Previous setups have tended to use collimated light, necessitating the use of huge optical elements for large targets. By changing the microscope objective and the camera lens, the field of view can be zoomed to accommodate objects of various sizes at various ranges. With enough laser power, a widely diverging beam can always be used and the zooming action can be accomplished solely with a telephoto zoom lens. This power could come from an optical amplifier of the sort currently under development at Lincoln Laboratory, which would output a few watts given a few milliwatts from the Nu Focus laser.

A photograph of one incarnation of the prototype system is shown in Figure 2-5.

2.3 Detector

A widespread and familiar detecting scheme for speckle measurement is an off-the-shelf CCD camera. Our choice was a Pulnix TM-9700 because it is fairly sensitive, its integrating time can be controlled for increased sensitivity, it has a digital output with progressive scanning, and it will support video bandwidth. One shortfall of the TM-9700 is its non-square pixels which are 11×9 μm. Square pixels are preferred but no cameras with the right combination of other features had them when we gathered the main elements for the system.

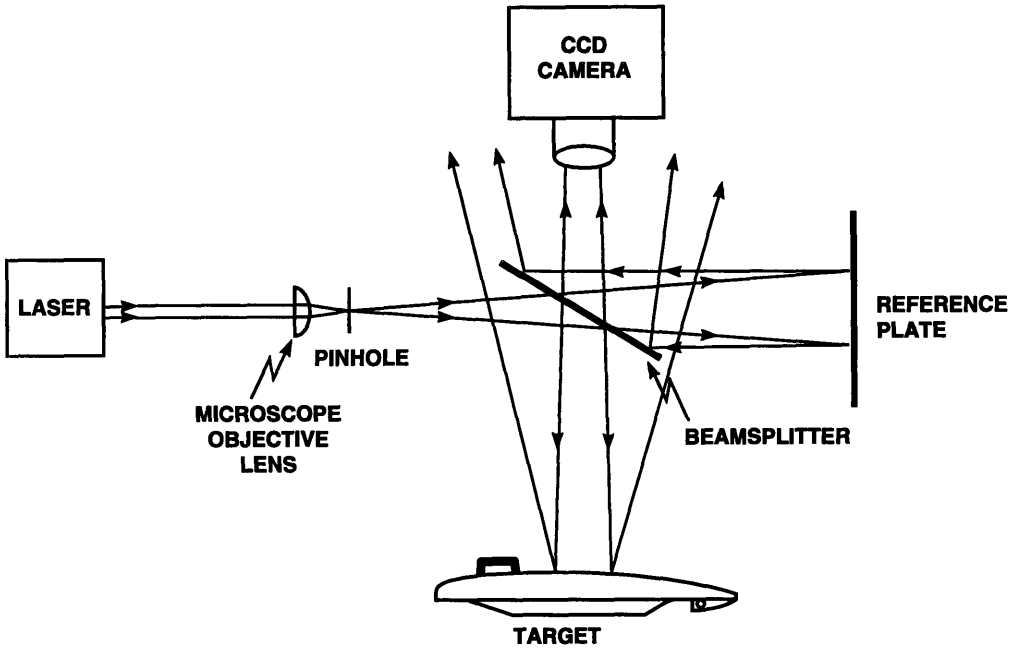

Figure 2-4: Optical schematic of the prototype 3D scanner.

2.4 How does it work?

The picture to keep in mind when thinking about this scanning configuration is schematically given in Figure 2-6. Light traveling directly from the source has a phase at the reference plate, $\Phi_{reference}$, given as

$$\Phi_{reference} = 2\pi \frac{R_{reference}}{\lambda} \tag{2.1}$$

in terms of the wavelength, λ, and the range from the laser (or camera) to the reference plate, $R_{reference}$. Light from the source reflects off the target and reaches the "virtual" reference plate (as shown in Figure 2-6) on the return trip with phase Φ_{target}:

$$\Phi_{target} = 2\pi \frac{R_{reference} + 2R_{difference}}{\lambda}. \tag{2.2}$$

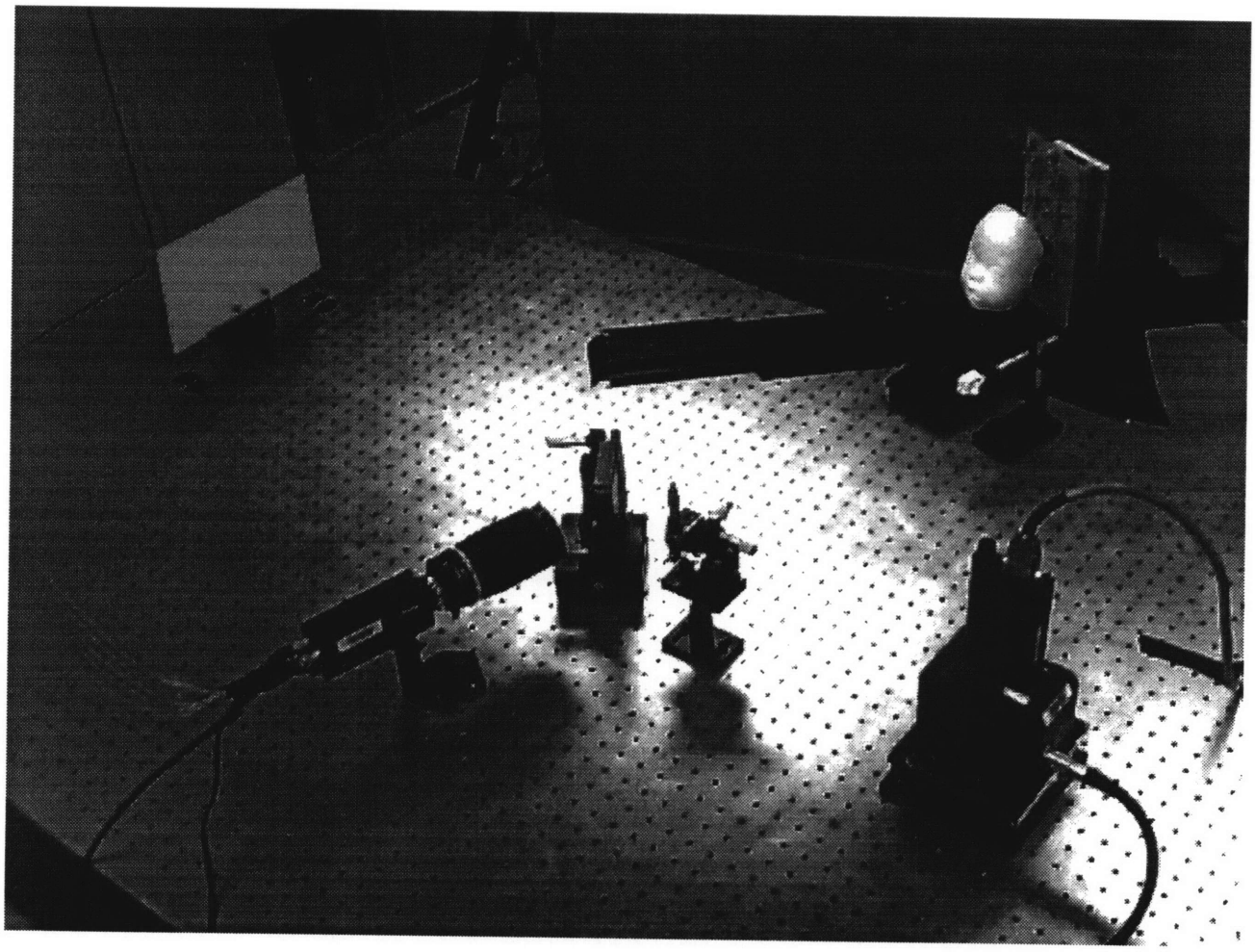

Figure 2-5: Photograph of the 3D scanner. In the lower right is the laser source which is aiming at the microscope objective and the pinhole. The diverging beam strikes the reference plate shown in the upper left along with one of the several targets arranged in the upper right. The CCD camera (lower left) detects the interference patterns.

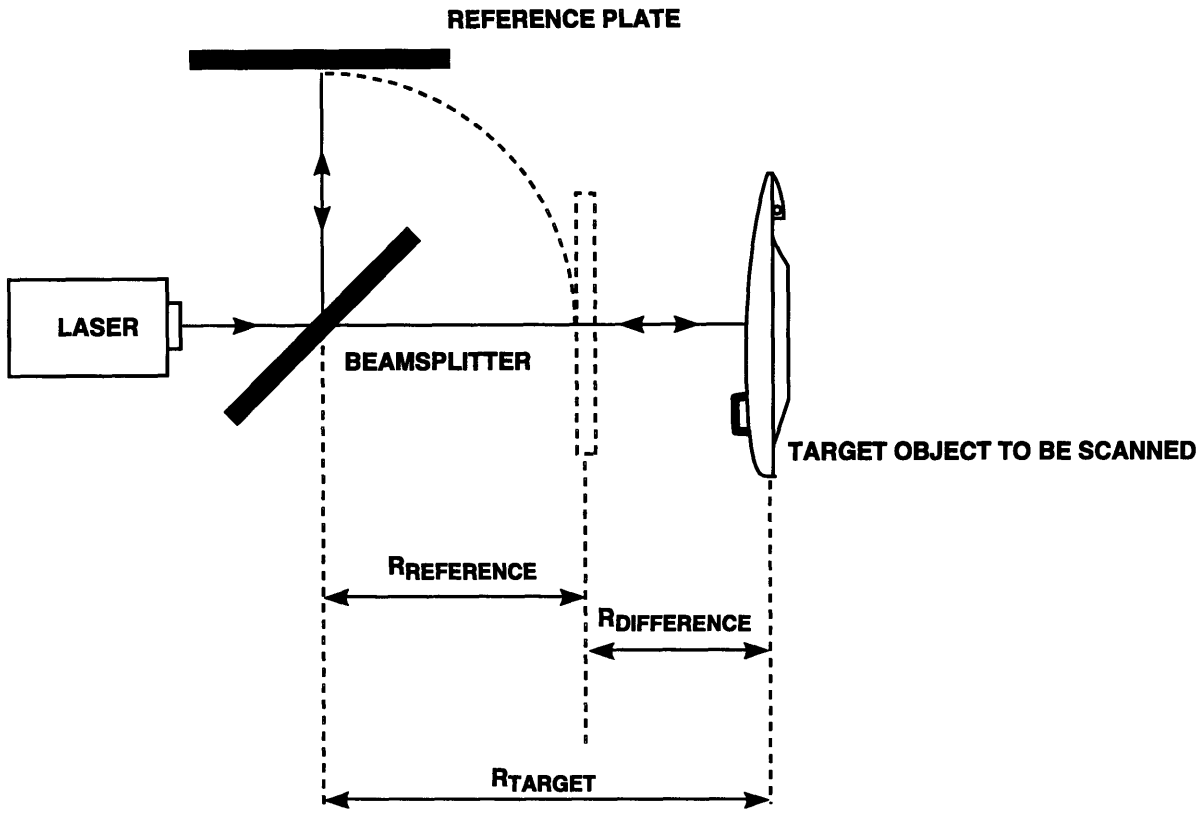

Figure 2-6: Diagram showing how the reference plate can be thought of as being in front of the target.

The phase difference at that range is just $\Phi_{difference}$:

$$\Phi_{difference} = \Phi_{target} - \Phi_{reference} \tag{2.3}$$

$$= 2\pi \frac{2R_{difference}}{\lambda}, \tag{2.4}$$

and that difference is propagated back to the camera from both light paths causing interference at the plane of the detector. A phase difference equal to an integer multiple of 2π results in constructive interference while half-integer multiples yield destructive interference. To get full modulation, it is helpful to match the reflectivity of the target with that of the reference plate.[1]

Our goal is to measure the range to the surface of the object, and our approach is to change the phase difference so that the detector registers an intensity fluctuation in response to our stimulus combined with the range information we seek. That is where tuning the laser fits in. By changing λ, $\Phi_{difference}$ moves in a way that depends on $R_{difference}$, the difference between the camera's (known) range to the reference plate and the camera's (unknown) range to the target's surface.

The mode in which the interferometer is operated during a 3D scan of an entire surface involves tuning the laser wavelength in time and simultaneously recording intensity images evenly separated in time. Thus, there is a known wavelength difference between consecutive frames. The number of oscillations of a pixel's intensity as a function of time is calculated for each pixel. That number is combined with laser wavelength information to produce a range value for the patch of the target's surface corresponding to that pixel using the relationship:

$$R_{target} = R_{reference} + m\frac{{\lambda_0}^2 - \lambda_0 \Delta\lambda_{total}}{2\Delta\lambda_{total}}, \tag{2.5}$$

which gives the range to the target surface, R_{target}, in terms of the number of oscillations, m, the starting wavelength, λ_0, the tuning range, $\Delta\lambda_{total}$, and $R_{reference}$,

[1] I coated the targets shown in Chapter 4 as well as the reference plate used with those targets with the same white spray paint to assure approximately equal return from the two legs of the interferometer.

all of which are known. (See Appendix A for a derivation.) Combining processed information from every pixel provides a complete surface contour.

Chapter 3

Datapath and processing engine

The measurement is completely under software control. A program running on a Sun Sparc 2 workstation commands the PM-5000 driven laser tuning mechanism, and speckle data are simultaneously captured by a DSP board interfaced both to the camera and to the workstation. Figure 3-1 schematically shows the system elements and their interconnections.

A user interacts with the system exclusively through an XToolkit application running on the Sun.

3.1 Computer hardware

3.1.1 Prior timescales

The scanner was intended to be high-speed in comparison with other 3D scanning technologies as well as in comparison with the Laser Speckle Laboratory's previous setup. The old acquisition scheme was plagued by various I/O bottlenecks. Thus, acquisition would take between 20 minutes and 8 hours, depending on the length of the scan, the amount of the data retained, and the mood of the laser. Processing was performed on a Sparc 2 workstation of the sort that serves as my host machine. The machine is measured to be slower than the DSP by over an order of magnitude. Finally, the processing steps were not fully automated but instead were often manually

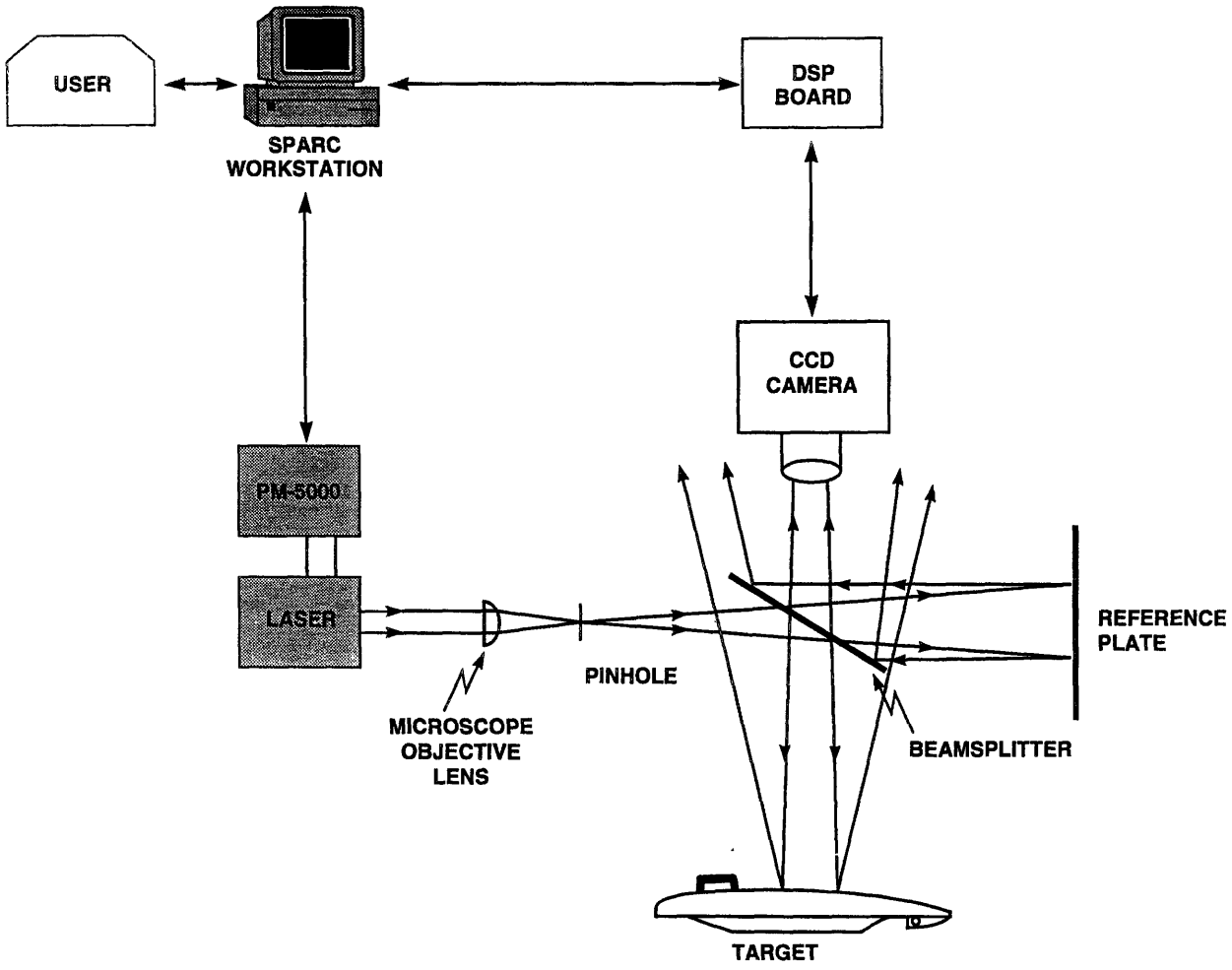

Figure 3-1: Schematic diagram showing the system elements and their interconnections.

directed in MATLAB or some such analysis software.

3.1.2 Original engineering

I designed the DSP board to be a processing element in a multicomputer under development at the Laser Speckle Laboratory, the Leonardo DSP Engine. The board carries a 40 MFLOPS processor, addresses up to 32 megabytes of DRAM, and routinely maintains an I/O bandwidth exceeding 2 gigabits per second without loading the processor. The single board executes the computation for a run over 10 times faster than the host machine (the same source code was used for this comparison) and is thus judged to be an important system element.

A second circuit board was put together to convert the IEEE digital video output of the camera to the protocol used in Leonardo.

The pair of original boards was connected to the host machine using André DeHon's SBus I/O card, originally designed for the Transit multicomputer.

3.2 The software front-end

After positioning one's part in the beam-path, the user is presented with a graphical user interface (GUI) on the X Windows workstation. The main control panel is shown in Figure 3-2.

I wrote the interface in the C programming language in conjunction with the XToolkit. It appears to function correctly under X11R5 as well as X11R6.

3.2.1 Main control panel

Display area

The central feature of the display is a 512×512 tv widget where images are rendered. Images are either intensity frames (as in Figure 3-2) from the camera or height-as-intensity frames from the DSP.

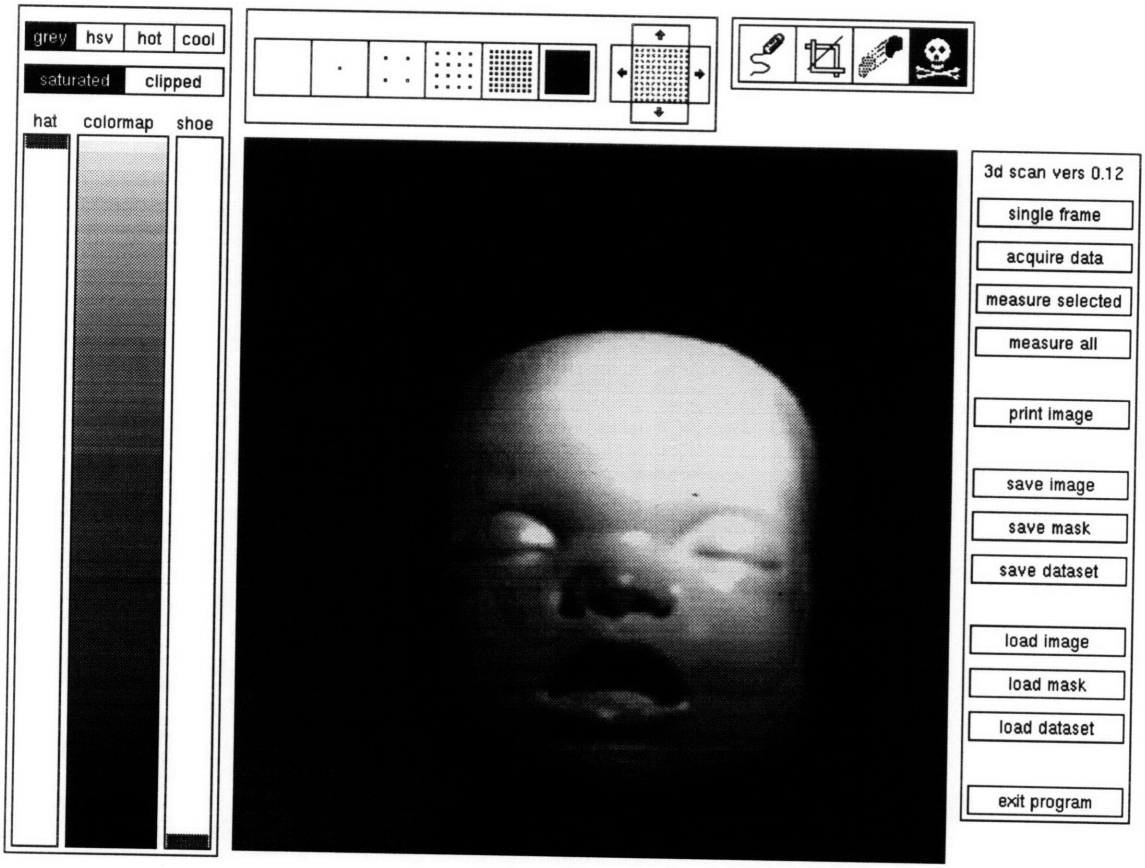

Figure 3-2: X Windows control panel for the prototype scanner.

Colormap widget

The colormap of the central image can be manipulated to give the user a clear idea of what he is looking at and where, within the scope of ranges or intensities registered by the scanner, the data fall. A colormap widget (on the left of the display) was engineered both as a control, giving the user instantaneous command of the image's appearance, and as an indicator, useful to quickly assess various settings of the scanner. The user might find that all of the values of an intensity frame fit within the bottom quarter of the colormap's height, for example, and consequently decide to integrate in the camera four times longer per image.

Drawing tools

Sometimes a user might wish to select some region or set of regions of the field of view to scan. For example, in an industrial situation, one might only need to check the heights of a few points on the target to satisfy a quality-control threshold. For these cases, a poor-man's drawing widget was written and added (in the upper right hand corner of the main display window) to draw and edit polygons and curved outlines in the image display area. The user selects one of the drawing or editing tools and marks out a region of interest. Connected paths are filled with some sampling matrix, selectable in the fill-pattern widget to the left of the drawing tools. The selected pattern fills the shape or set of shapes drawn with the drawing tools indicating that those points are selected to be measured by the scanner. When undersampling a surface, the sample grid can be shifted around by a tool on the right of the fill-pattern widget added to let the user align the sampling pattern with details on the image.

Control plug-in

The parts described above form a structure within which several speckle-based measurements fit nicely. The image plane technique discussed here calls for a few additional control buttons. Other techniques call for different controls. Therefore, the

user-interface was designed to accept experiment-specific control panels (which appear to the right of the tv widget in the interface) as modular plug-in units.

The control plug-in for image-plane 3D scanning is very simple. The user has twelve options with this plug-in:

Single frame: The "single frame" button takes a single frame from the CCD camera and displays it in the image area. This is useful to check light levels (through the use of the colormap widget) and to aim the camera.

Acquire data: The "acquire data" button sends the laser scanning and stores 256 consecutive images in the memory of the DSP board. The process takes a little over 8.5 seconds and is limited (for the scans shown in chapter 4) by the camera's thirtieth-second integration time per frame necessary with the maximum output power of the Nu Focus laser.

Measure selected: If the user needs to measure the heights of only certain regions of the camera's field of view, or if he wishes to undersample the array by some factor, he can select a set of points using the drawing and filling tools discussed above. Then, after acquiring a dataset, the "measure selected" button sends requests to the DSP board to process data vectors corresponding to the selected pixels. When the processing is complete, a separate display window is spawned (shown in Figure 3-3) which contains a mesh-plot of the surface heights.

Measure all: The "measure all" button does the same thing as "measure selected" would if the user selected the whole frame. A $256 \times 256 \times 256$ point dataset is analyzed in under 60 seconds with the single DSP currently installed.

Print image: Postscript output of the current image displayed in the tv widget is generated and spooled to the default network printer when the "print image" button is clicked on.

Save image: This button creates a file containing image data in ascii format.

Save mask: "Save mask" creates a file with a representation of the polygons and curved outlines currently drawn on the image. The outlines can be reloaded by the "load mask" button. This feature might be useful to someone who routinely measured a handful of different parts.

Save dataset: To save the entire set of 256 frames each containing 256 × 256 pixel values of 8 bits each to the workstation's mass storage device for later processing, press the "save dataset" button.

Load image: "Load image" renders an image from disk to the tv widget.

Load mask: See "save mask" above.

Load dataset: This button uploads a dataset into the memory of the DSP board.

Exit program: "Exit program" cleanly terminates the user interface program along with all of its children.

The mesh display window (Figure 3-3) gives the user the ability to navigate around and zoom into the mesh plot. Additionally, the data can be exported from this window in 2D form in Postscript or in 3D form in the DXF file format. DXF is the industry standard file format for representing objects in three dimensions and DXF files can be imported into most mechanical engineering CAD tools as well as 3D rendering computer graphics software.

3.3 What happens behind the scenes

3.4 Processing

Once a dataset is in the memory of the DSP board, the host machine can request that the height of some set of pixel locations be extracted from that dataset. The vector of 256 pixel values (corresponding to the intensity of some location as a function of time) are sent through a Fast Fourier Transform (FFT). The index of the peak in the

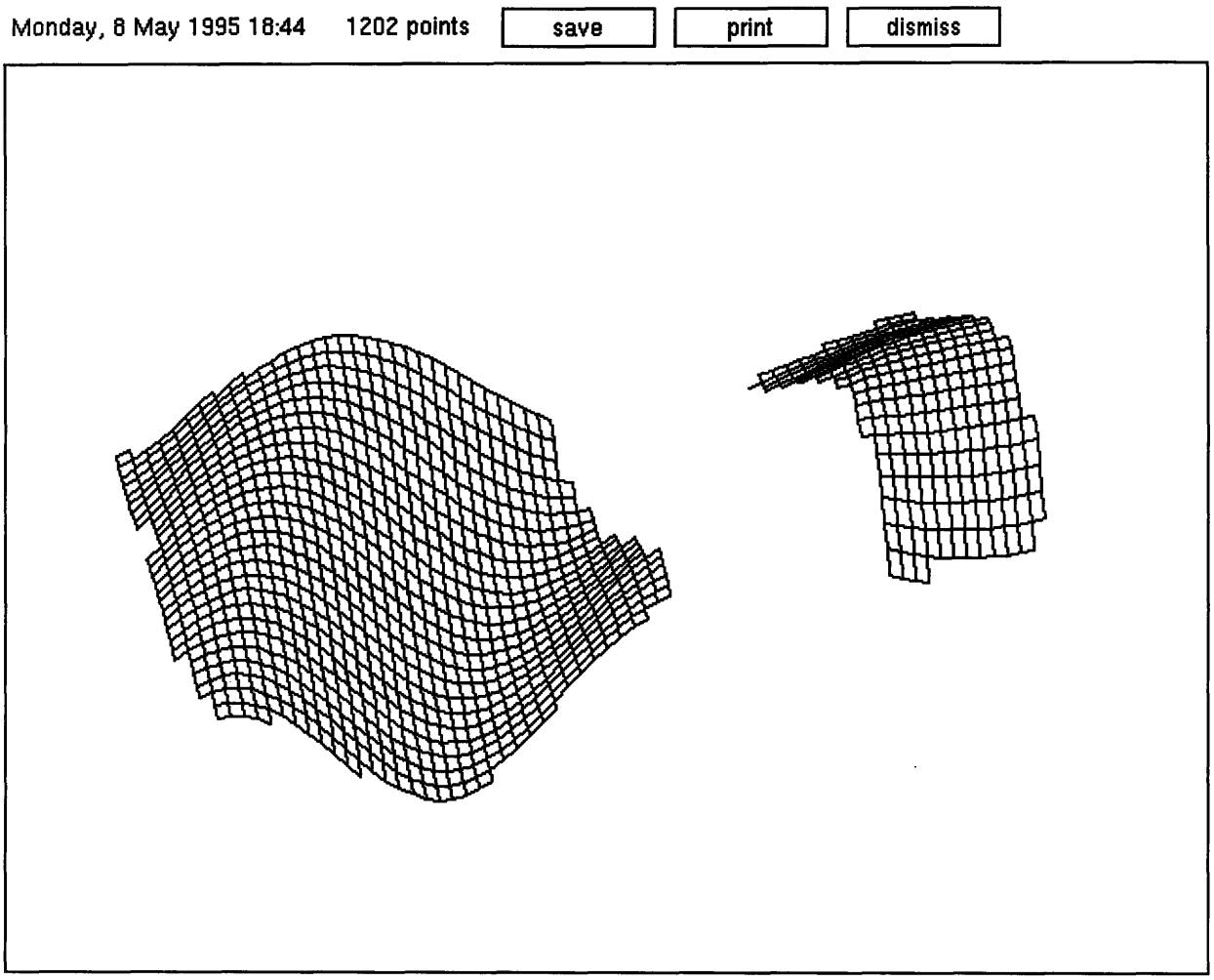

Figure 3-3: Measured data pop up in this window when "measure selected" or "measure all" buttons are pressed. In this example, the user selected two regions of the frame to measure and clicked on "measure selected."

spectrum computed by the FFT essentially gives the number of intensity oscillations in a somewhat noise-immune way. That value is combined with the run parameters and equation A.8 to get a value for the distance to the object.

3.5 Postprocessing

It is the nature of speckle scanning that some pixels will be more fully modulated than others. Furthermore, at low light levels, camera noise and small amounts of ambient light can mask out the modulation from the scanning laser. Both of these conditions lead to weak spectral peaks and potentially incorrect data extraction. To smooth out noise of this sort, median filtering is sometimes used to evaluate the feasibility of a pixel's range considering the range of its neighbors. This is the first point in the computation at which neighboring pixels share information.

I have found that plenty of light (almost saturating the CCD) is best for minimizing the noise in a 3D measurement.

3.6 The potential for increased parallelism

In the last section, I pointed out that information from a given pixel need not mix with information from other pixels until late in the measurement, and even then, mixing only occurs within a local neighborhood of the pixel. Therefore, this is a computation that begs to be parallelized. Chapter 5 gives motivation to increase the number of processors to equal the number of pixels.

Another way to exploit the distributed nature of the imaging scheme is through the use of multiple cameras. Each camera would stare through its own beam-splitter, providing a simultaneous view of the target and the reference plate.

Applications of this feature are easy to think of. In inspecting a car door on an assembly line, for example, one might want to have the laser flooding the entire surface with light and have one camera with a wide field of view measuring the overall shape of the door and another with a tight zoom on the handle indentation to make

sure that the lock mechanism will have a precise fit. Applications of fovial vision have found their place in the 2D imaging world, and this technique allows for carry-over into 3D imaging.

Chapter 4

Data

This chapter presents three recent datasets from the prototype.

4.1 Resusci-infant

The detachable face of a Red Cross CPR practice mannequin, Resusci-infant, was scanned. The face is the actual size of an infant's: about 9×10 cm.

4.1.1 Inapplicability of traditional techniques

There are a few characteristics of this object that constitute challenges to other 3D scanning technologies.

Soft and flexible material

Resusci-infant was engineered to feel like a baby to provide a realistic training tool for CPR students. Thus, the face is soft and flexible. A CMM would deform it during a scan and therefore provide a useless measurement.

Deep well of the mouth

Triangulation techniques are only effective on surfaces that can be illuminated from a much different angle from the angle to the detector. Therefore, deep wells, such as

Figure 4-1: 2D image of Resusci-infant's detachable face with normal overhead lighting

the cavity of Resusci-infant's mouth, are not gracefully dealt with by triangulation scanners.

4.1.2 2D data

Figure 4-1 is a photograph of Resusci-infant's detachable face taken right before the run. The photograph was taken with the scanner's camera with the room lights on and a black felt cloth covering the reference plate. The laser was switched off.

Figure 4-2 is a frame taken after switching the laser on, removing the felt covering the reference plate, and turning off the room lights. Notice the noisy appearance of the image. That noise is always present when imaging using coherent radiation—it

Figure 4-2: 2D image of Resusci-infant's detachable face illuminated with 780 nm laserlight.

is called laser speckle [20]. The pattern of speckles appears to twinkle as the laser is tuned. That is the source of all the 3D information used in our measurement.

4.1.3 3D data

The face is 10 cm deep. Therefore, using Equation A.7, the laser was scanned from 780.0 nm to 779.5 nm to give 128 range cells that cover the target's range plus a bit more (to compensate for my casual alignment job).

The steps outlined in Chapter 3 were taken with this dataset. Namely, I positioned the face in front of the camera and focused. I took an intensity image with "single frame" and then selected a region of interest from within the frame. Then, I clicked

on "acquire data" and "measure selected." From the pop-up, I exported the 3D data to a commercial graphics program.

A contour plot of the face was generated with adjacent contour lines indicating a height difference of one range cell, about 791 μm. That plot is shown in Figure 4-3. Notice that all of the facial structures are well resolved.

Figure 4-4 is a more attractive way of visualizing the data. It is a ray-traced rendering of the surface viewed from the baby's lower right. Notice how clean the nose and mouth as well as the closer cheek and eye are. The forehead, however, while the right shape, has a more bumpy texture than expected. Comparison of Figure 4-1 and Figure 4-2 reveals the cause of the signal degradation—namely that the forehead was poorly illuminated by the laser and more light was needed in that area. I included this dataset as an example of the merits of ample illumination and of the noise arising from its absence.

4.2 Analog printed circuit board

Part of an analog printed circuit board was scanned as well. The target was chosen for several reasons. First, it is an order of magnitude smaller in range than the face of the above section: the tops of the capacitors are very nearly 1 cm from the front of the board. Second, it is a complex surface with many more features than the face and therefore my often overpowering temptation to broadly smooth the dataset is absent here.

The laser tuning range was increased for this dataset to reduce the 791 μm range-cell size to one tenth that value.

White spray paint was used to reduce the contrast in intensity as well as in diffusivity among the various sruface-types on the board. With enough laser power and a detector with enough dynamic range, the paint would probably be unnecessary.

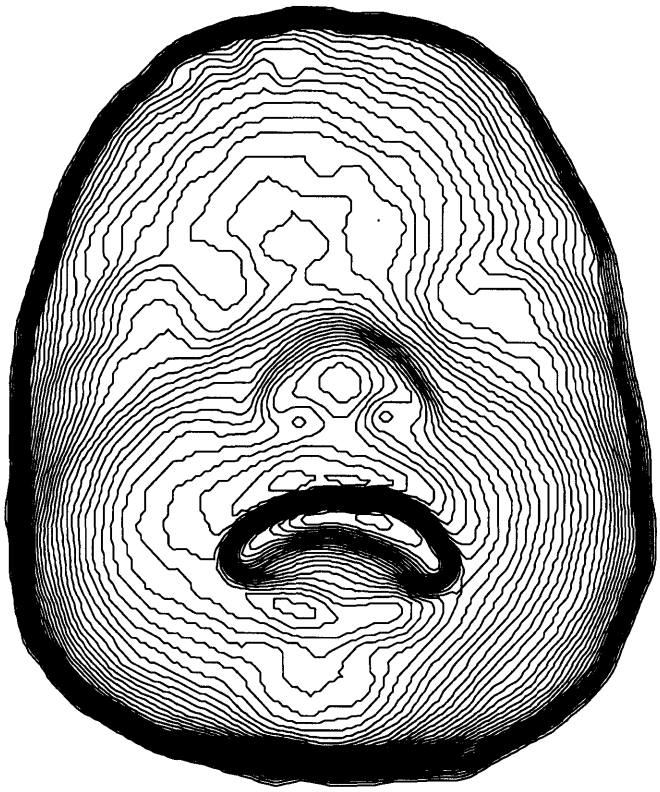

Figure 4-3: Contour plot of Resusci-infant's detachable face. Contours are separated by about 791 μm in height.

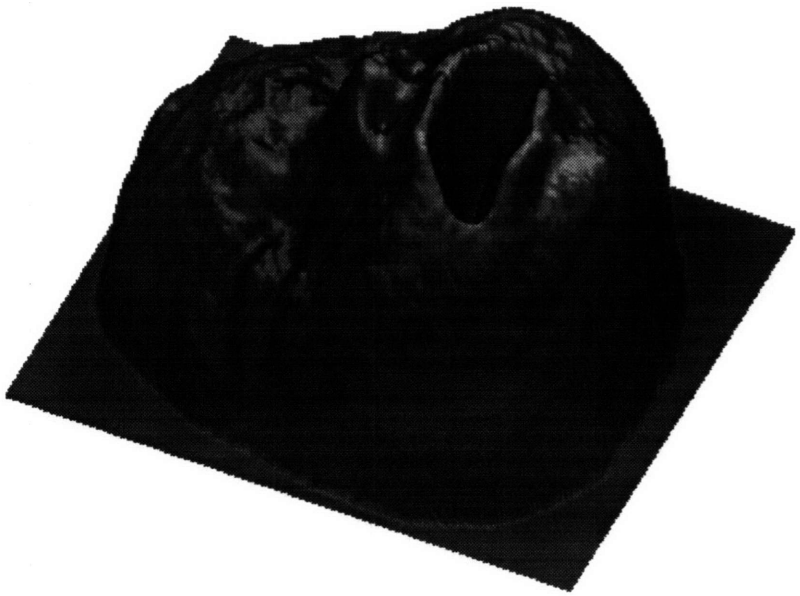

Figure 4-4: Computer reconstruction of Resusci-infant's detachable face from a different view from the one seen by the camera.

4.2.1 2D data

Figure 4-5 shows the camera's view of the printed circuit board from a range of 65 cm. As with Figure 4-1, the room lights are on, the laser source is off, and the reference plate is covered with a black cloth. The two chips shown are standard 300 mil dip's with pin spacings of 2.54 mm.

4.2.2 3D data

Figure 4-6 is a ray-traced rendering of the surface height function measured by the prototype.

4.2.3 Practical application

One can imagine a quality-control system to check that all of the circuit elements are placed in a board like this one. With 3D data such as that shown in Figure 4-6, many of the common ambiguities that make the problem difficult are absent. Thus the system could be quite robust and trustworthy.

4.3 Calibration

4.3.1 Quantitative characterization of speckle scanning

A mechanical engineering graduate student in the Laser Speckle Laboratory, Joe Karlin, is responsible for a calibration of the laser frequency as well as a quantitative comparison of laser speckle to other systems, particularly coordinate measuring machines. The reader is referred to his thesis [2] (currently in progress) for this sort of analysis.

In place of a complete characterization, I include a consistency check, to demonstrate that the system behaves as expected.

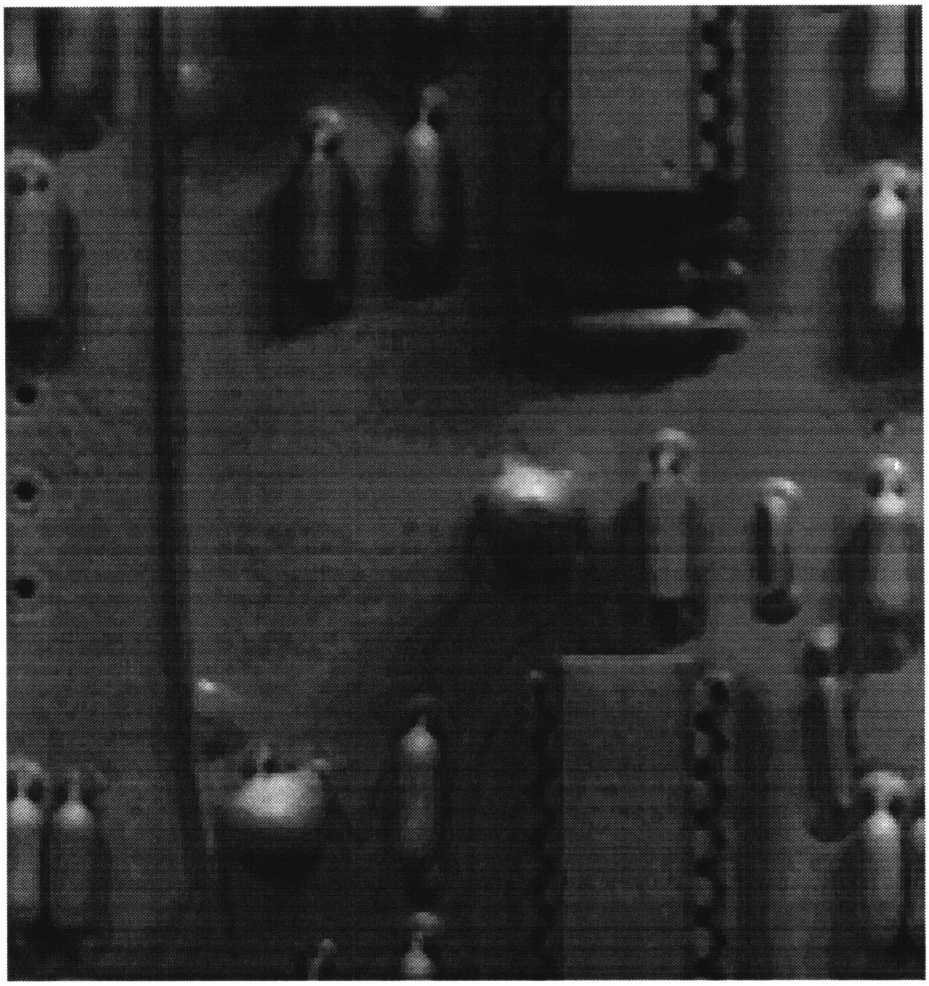

Figure 4-5: Photograph of a printed circuit board.

Figure 4-6: Ray-traced rendering of the printed circuit board's height function measured by the prototype.

4.3.2 Consistency check

Figure 4-7 is a photograph of a nine-step target a few centimeters in each dimension. The target was scanned by my prototype. 3D data from that scan were fit to equations representing nine planes with undetermined heights and pitches plus a few additional degrees of freedom to allow the planes to connect on their edges. A rendering of that fit is shown in Figure 4-8.

The best fit number of oscillations observed at the range of each of the nine upward-facing surfaces was plotted against the height of those surfaces measured with a machinist's caliper. The nine datapoints were best fit with a line of slope 5.7 oscillations per mm. The plot is shown in Figure 4-9.

Run parameters suggest that the laser was scanned from 780.0 nm to 778.5 nm. This would be consistent with counting an oscillation for every 202.4 μm of range, or 4.9 oscillations per millimeter.

The discrepancy between a predicted slope of 4.9 and a measured one of 5.7 can be attributed to poor knowledge of the laser frequency (due to the continued use of calibration tables generated before a major overhaul of the laser head) and to a possible mis-alignment of the reference plate (which may not have been exactly perpendicular to the beam striking it). The discrepancy is not so large, on the other hand, that it might indicate a flawed understanding of the physics or of the apparatus.

Figure 4-7: Photograph of a nine-step target used as a consistency check.

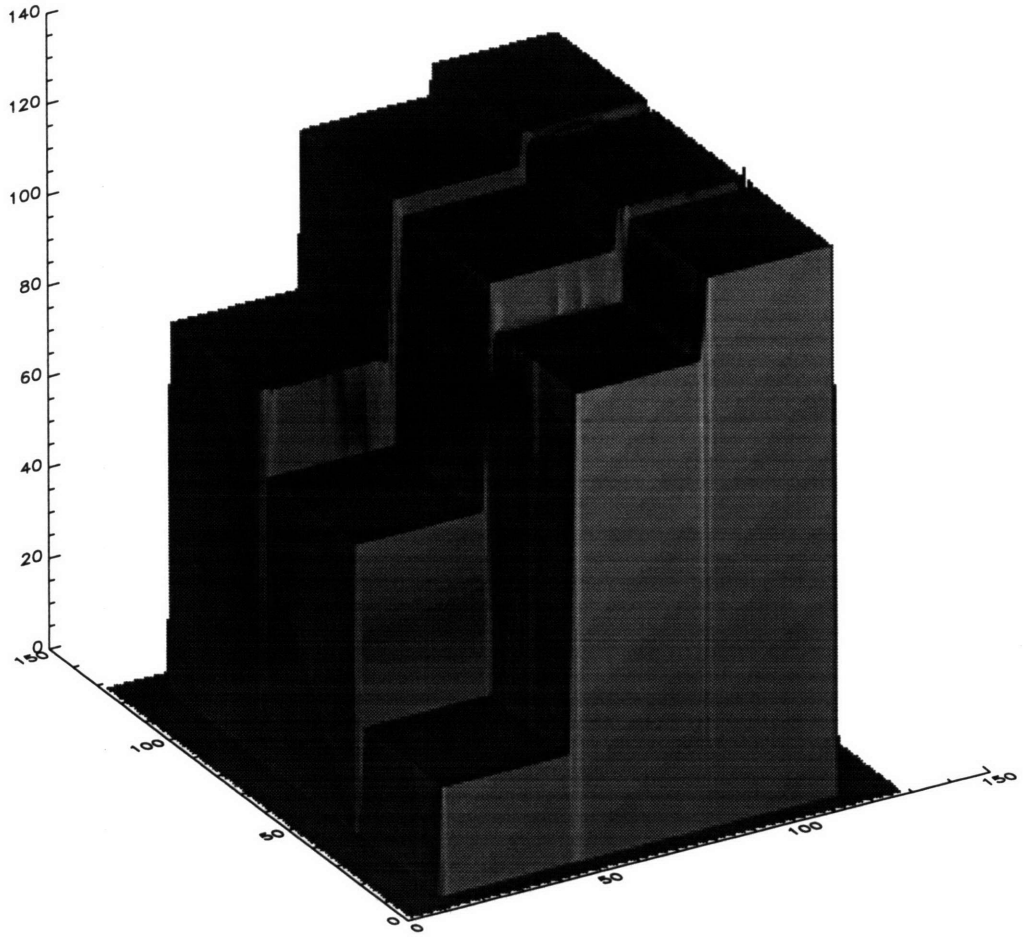

Figure 4-8: Ray-traced rendering of nine-step 3D data fit to a model of the nine-step target.

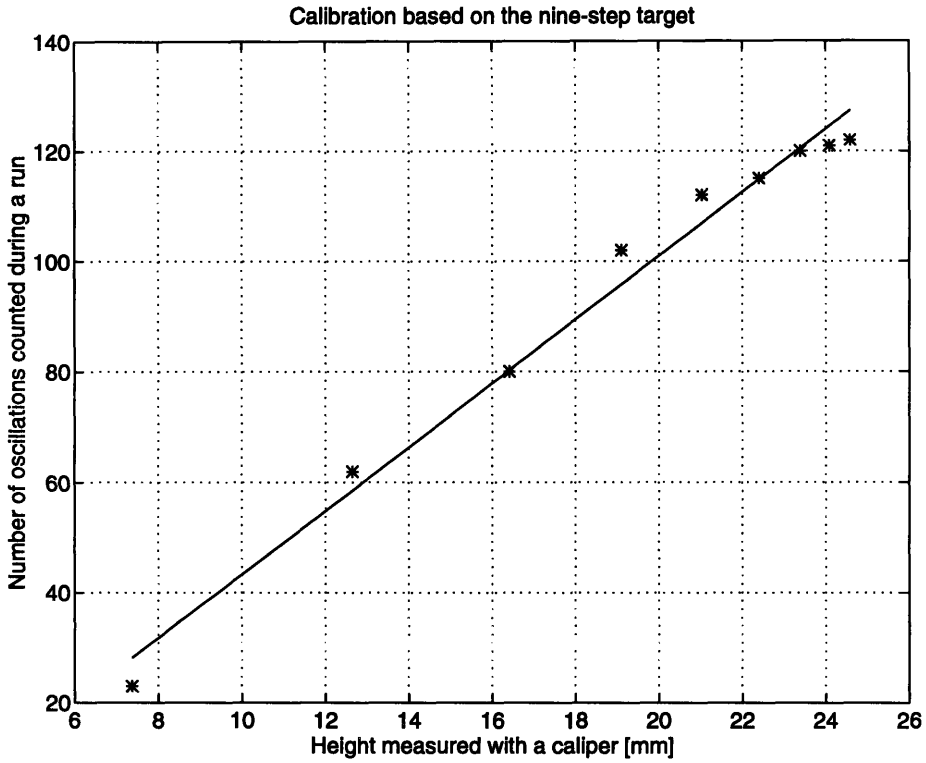

Figure 4-9: A comparison of the speckle-based measurement and measurements made with a machinist's caliper.

Chapter 5

Feasibility of 3D video

One of the exciting possibilities with this 3D imaging scheme is that it can be sped up to video rate by engineering that doesn't at all stretch the bounds of today's technology.

5.1 Technical steps toward video-rate 3D acquisition

There are three basic ingredients in measuring an object in the current implementation: a laser that scans through some tuning range during a measurement, a camera that observes the intensity fluctuations on the surface of the object, and a processing element to asses the frequency of these fluctuations. Somehow, these ingredients must be individually sped up or replaced by faster elements.

For this discussion, I will consider the ability to generate 30 "3D frames" per second from realtime data to be "3D video."

5.1.1 Tunable Laser

Somehow, a detector must, in one thirtieth of a second, observe a comparable number of intensity oscillations to the number seen in eight seconds during a run on my prototype. This requirement has two ramifications: first, the laser scan must be sped

up by a factor of the measurement speedup—240 times. Second, the laser power must also be scaled by 240 so that the detector can have the same number of photons per measurement as was just sufficient before.[1]

Laser speedup

As discussed in chapter 2, the Nu Focus laser used in the prototype equipped with a PM-5000 linear driver is capable of tuning at very high rates. In fact, for the data assembled in chapter 4, the PM-5000 was scanning nearly two thousand times slower than its maximal rate. Therefore, the factor of 240 is well within the capabilities of the current system.

However appropriate this mechanical system may be for a laboratory situation, the assembly may be unnecessarily robust and too expensive for a market or industrial context. The mechanical problem to solve is translating a mirror about three millimeters at 30 Hz with an accurate sawtooth position-time dependence. Known solutions to this problem include the use of hi-fi long-throw woofers such as those manufactured by Paradigm among others. Depending on the error tolerance allowable by the scan resolution required, a Mossbauer motor as used in Mossbauer spectroscopy might be necessary. If higher repetition rates are required, for example thousands of "frames" per second, three millimeters may be too long to throw without distortion for higher-frequency actuators based on the same speaker technology. For this generation of scanners, a cam machined with an Archimedes' spiral can be spun while in contact with the spring-loaded mirror mount of the laser cavity.

Increasing the laser power

In chapter 2, I mentioned that optical amplifiers exist that can boost the output power of the diode laser by a factor of a thousand. Such a factor could be shared between scanning larger surfaces and scanning faster. For example, a scan of a surface four times the area of the full-face data in chapter 4 could be viewed at full 30 Hz frame

[1]Increasing the laser power is a known possibility and thus is more feasible than finding or developing a detector array with substantially more sensitivity than the one used in the prototype.

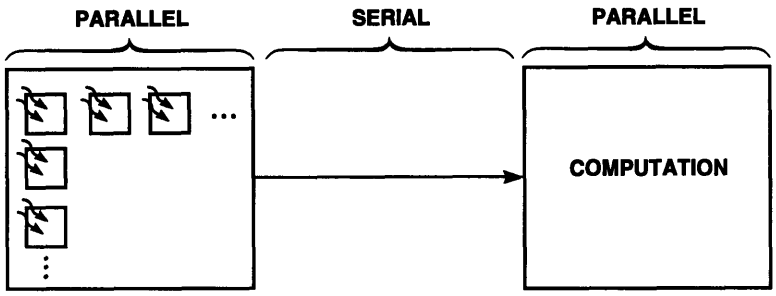

Figure 5-1: Data from an array of detectors are serially transferred to a parallel computation unit.

rate if a laser amplifier were used with its maximum gain. Further, an area twelve times that of the face could be scanned at 10 3D fps.

It should be mentioned that even though a total laser power of several watts is sufficient to burn skin if concentrated in a tight beam, spreading that power over a large surface area reduces the energy density in correspondence with that spread and therefore diminishes the risks associated with laser sources of that power.

5.1.2 Detection and processing

The prototype system was built mostly with off-the-shelf components. Consequently, camera data are serialized and transmitted to the processing elements through a severe bandwidth bottleneck. Figure 5-1 illustrates the problem. Reading CCD arrays out a very high speeds induces an unacceptable amount of noise for many applications. Therefore, high speed CCD arrays are now built with multi-port readout to alleviate this shortcoming of most cameras.[2] Nonetheless, since (for our application) each pixel

[2]Lincoln Laboratory is currently developing four-port CCD's, for example.

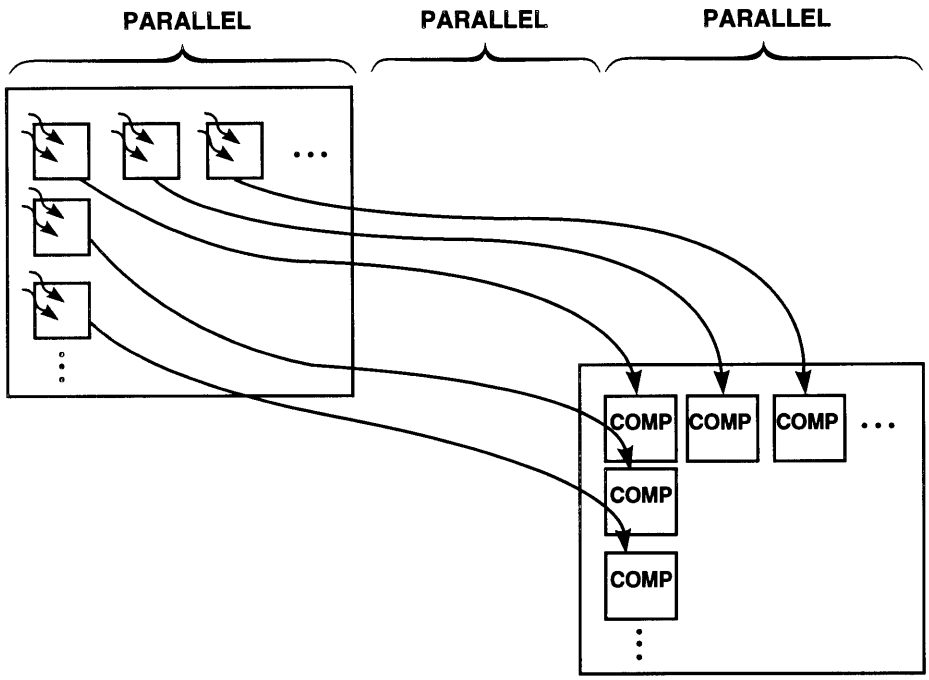

Figure 5-2: Data from an array of detectors are transferred in parallel to a parallel computation unit.

is treated independently until somewhat late in the computation, any serialization (even if shared by a handful of ports) can be considered wasteful if done too early. Ideally, then, one is driven to place elements responsible for the computation of frequency content in parallel communication with the pixel intensity output as shown in Figure 5-2. An actual sensor could be built as illustrated in Figure 5-3. The sensor consists of an array of photo-detectors coupled individually to computation units which I currently envision as analog frequency-to-voltage converters or binary counters. The computation units are linked horizontally in shift registers like the photo-detectors in a CCD. The whole array could be integrated on a single chip or, in some prototyping stage, could be implemented on a high-density surface-mount printed circuit board.

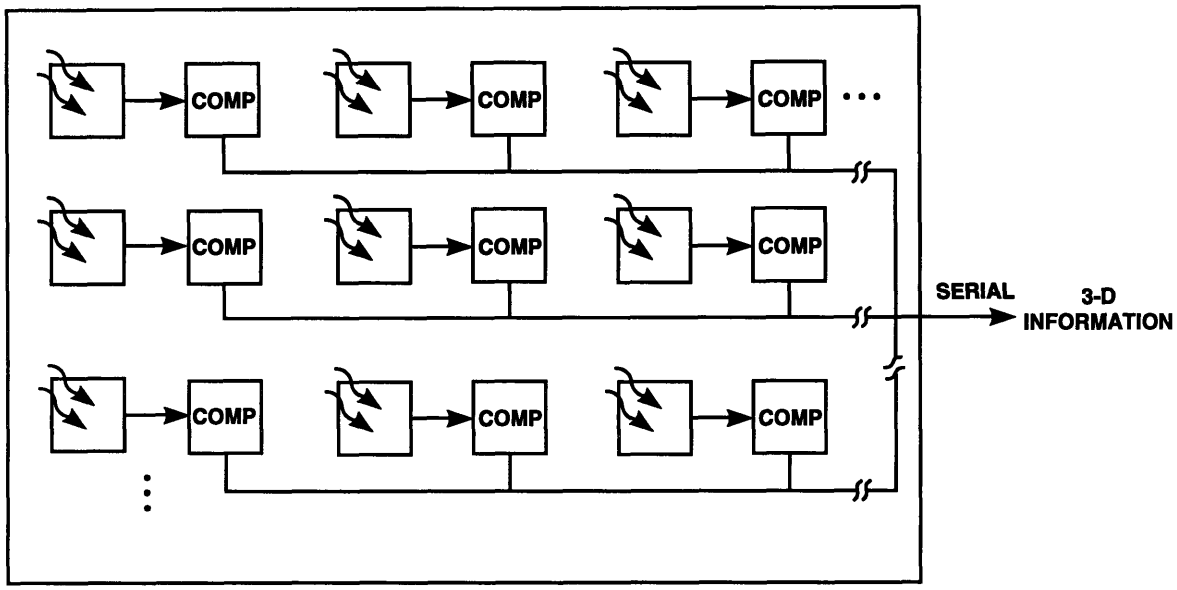

Figure 5-3: An array of computation units integrated with photo-detectors to make up a parallel sensor suited for 3D scanning applications.

Frequency-to-voltage converters

Frames read out of the chip or board would consist of voltages proportional to (or identifying of in some other way) the fundamental frequency of intensity oscillation detected by the sensor. Frequency-to-voltage converters are well understood and used in an abundance of existing applications in the frequency range needed, i.e. 30 measurements per second $\times$ hundreds of oscillations per measurement, or a few kilohertz. Furthermore, integrated photo-detectors generally have response well beyond the megahertz range.

Binary counters

Instead of turning to analog techniques, the frequency-to-voltage converters can be replaced by several-bit ripple-counters globally reset at the start of each measurement. Some analog interface from the photo-diode or photo-transistor would have to be worked out so that the counter is triggered only once per oscillation from the (potentially noisy) intensity signal. I expect that a Schmidt trigger with thresholds spaced off of DC an amount that slowly followed the AC-coupled power of that pixel would do the trick. Fortunately, real intensity data is available to me in abundance and so thorough simulation is possible for this part of the design.

Supposing that the photo-detector and analog interface had the (modestly projected) bandwidth of 10 MHz (and that there was no shortage of photons for a measurement). Then, in a thirtieth of a second, the counter will not exceed 333,333. So, for 19 bits of ripple-counting (at the cost of perhaps 4 μm^2 per bit in a modern technology such as Lincoln Laboratory's deep-UV process) we could find ranges to a part in a hundred thousand at video-rates.

The ability to count up to 2^{19} can also be exploited in long measurements. Suppose the laser starts at 780 nm and scans through 1 nm at whatever rate allows the counters to do their job. Then, (with the help of equation A.7) any surface within 159 meters of the reference plate falls into an acceptable range cell with no aliasing! Furthermore, the data give the position of the surface to the nearest 300 μm. One sees a meter-

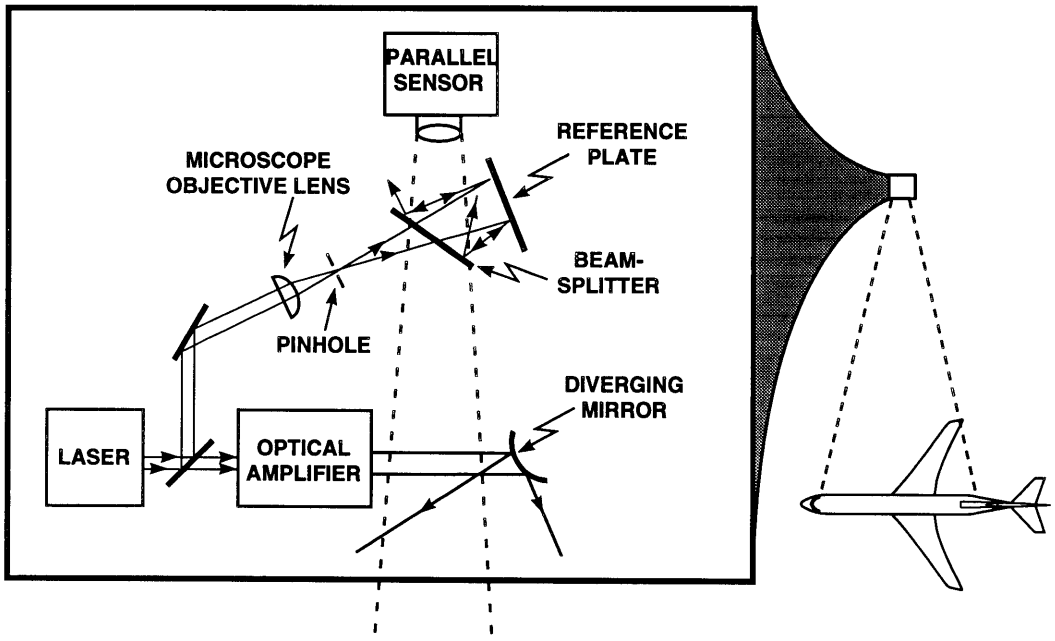

Figure 5-4: A system for large-scale or video-rate 3D scanning.

sized machine of the sort sketched in Figure 5-4 that can scan large scenes such as rooms and airplane wings. Notice, however, that with long measurements, vibration is potentially a much bigger concern than with extremely rapid scans.

5.2 Uses of 3D video

The ability to measure surfaces at video-rates brings to mind many applications. Consider these:

1. 3D medical endoscopy (through the use of fiber).
2. Measuring human body dynamics for physical therapy and sports.
3. Realtime range feedback sensors to allow blind individuals to "feel" remote objects to aid navigation and scene comprehension.
4. Studying the deformation of sheet-metal panels in automobile crash-tests to improve safety engineering.

5. Automating quality-control in assembly lines as well as sorting and handling of irregular objects such as mail parcels and fresh fruit on conveyer systems.

6. The source of material for computer-enabled 3D games, animations, and other "virtual reality" technologies such as virtual teleconferencing.

7. Wireless gesture-controlled computer interfaces.

Naturally, as with every such advance, once the technology exists the need for it will appear in a currently unimaginable set of industries.

Chapter 6

Conclusions

The 3D scanning technique based on image-plane laser speckle described in this thesis overcomes a number of the limitations of other technologies.

6.1 Speed

The only moving part in the whole scanner is a five gram mirror within the laser head. Furthermore, because of the mechanical design of the laser cavity, a simple motion of that mirror scans the laser frequency. Finally, sampling the image-plane interference pattern while the laser is tuning is demonstrated here to work. Therefore, with enough laser power, very high speed 3D scans are possible.

6.2 Size

The prototype scanner uses diverging laser light to generate its data. Therefore, a bigger scanner is not needed for bigger targets.

6.3 Robustness

The prototype design is monostatic. In other words, light headed toward the target returns along the same path to the camera. Thus, you can scan any surface that you can see.

6.4 The potential for automatic registration

Drawing tools to select regions of interest within the field of view of the scanner are possible because the same detector is used for intensity and 3D acquisition.[1] Speckle scanner software could be written for an industrial application that automatically registers a sampling pattern with the intensity image thus allowing the scanner to stare down on a conveyer belt and measure parts with haphazard orientation.

6.5 Future work

6.5.1 Processing

The FFT is easy to trust, but it comes with a computational tax that scales poorly as the number of range cells goes up. Some noise-robust time-domain counting scheme might be the right thing here.

Secondly, the median filter we used to patch over "drop-out" pixels, while repairing the surface of our reconstruction, reduces our cross-range resolution. An improved algorithm would weigh a pixel value against the value of its neighbors based on the height of the Fourier Transform peaks. Such an algorithm would tend to leave well established values alone and modify only "weak" pixels.

[1]Notice that other technologies lack this feature. Users of CMM's typically take tens of minutes to align parts on the stage. If similar parts are measured many times, a specialized jig is fabricated to mount the parts with precise registration more quickly.

6.5.2 Hardware

A good next step with the hardware would be to integrate an optical amplifier into the system to demonstrate the technique on large objects. Given the success of that demonstration, the next reasonable endeavor would be to develop the sensor proposed in section 5.1.2 to pave the way towards 3D video.

Appendix A

Count-to-range calculation

This appendix works out how to use a count of intensity oscillations to get the range to target. The argument goes along with Figure 2-6.

Consider the criteria for causing a maximally bright pixel to undergo m complete intensity oscillations, corresponding to m 2π phase shifts. Let n be the multiple of the first wavelength that just fits in the optical path-length difference $2R_{difference}$. Then

$$n = \frac{2R_{difference}}{\lambda_0}. \tag{A.1}$$

During a 3-D scan, we decrease the wavelength a total amount, $\Delta\lambda_{total}$. We count m intensity oscillations at some pixel during that scan, corresponding to a phase shift of $2\pi m$:

$$(n+m) = \frac{2R_{difference}}{\lambda_0 - \Delta\lambda_{total}}. \tag{A.2}$$

Writing

$$(\frac{2R_{difference}}{\lambda_0}) + m = \frac{2R_{difference}}{\lambda_0 - \Delta\lambda_{total}} \tag{A.3}$$

$$\frac{2R_{difference} + m\lambda_0}{\lambda_0} = \frac{2R_{difference}}{\lambda_0 - \Delta\lambda_{total}}, \tag{A.4}$$

we can then cross-multiply:

$$2R_{difference}\lambda_0 = 2R_{difference}\lambda_0 - m\lambda_0\Delta\lambda_{total} + m\lambda_0^2 - 2R_{difference}\Delta\lambda_{total}. \tag{A.5}$$

Then, solving for R_{target}, we have

$$R_{difference} = \frac{m{\lambda_0}^2 - m\lambda_0\Delta\lambda_{total}}{2\Delta\lambda_{total}} \tag{A.6}$$

$$R_{target} = R_{reference} + m\frac{{\lambda_0}^2 - \lambda_0\Delta\lambda_{total}}{2\Delta\lambda_{total}}, \tag{A.7}$$

which is an exact solution for the range to the target surface, R_{target}, in terms of m, λ_0, $\Delta\lambda_{total}$, and $R_{reference}$, all of which we know.

Bibliography

[1] F.S. Luecke, "Tuning System For External Cavity Diode Laser," U.S. Patent 5,319,668 (1994).

[2] J.H. Karlin, "3D Imaging Methods for Manufacturing, with Emphasis on the Laser Speckle Technique," S.M. thesis, MIT, Cambridge, MA (1995).

[3] L.G. Shirley, E.D. Ariel, G.R. Hallerman, H.C. Payson, and J.R. Vivilecchia, "Advanced Techniques for Target Discrimination Using Laser Speckle," Lincoln Lab. J., V. 5 N. 3 p.367 (1992)

[4] L.G. Shirley, "Laser Radar Applications and 3D Imaging," in *Tunable Laser Applications* ed. F Duarte, Marcel Dekker, NY (1995).

[5] P.J. Besl, "Active Optical Range Sensors," in *Advances in Machine Vision* ed. J.L.C. Sanz, Springer-Verlag, NY (1989).

[6] *MicroVal PFx User's Manual*, Browne & Sharpe Mfg. Co, North Kingstown, RI (1991).

[7] M. Takeda and H. Yamamoto, "Forier-transform profilometery: three-dimensional shape measurements of diffuse objects with large height steps and/or spatially isolated surfaces," Appl. Opt. 30, 7829 (1994).

[8] N. George, "The Wavelength Sensitivity of Back-Scattering," Opt. Commun. 16, 328 (1976).

[9] N. George, "Speckle from Rough, Moving Objects," J. Opt. Soc. Am. 66, 1182 (1976).

[10] N. George, A.C. Livanos, J.A. Roth, and C.H. Papas, "Remote Sensing of Large Roughened Spheres," Opt. Acta 23, 367 (1976).

[11] N. George, "Speckle," SPIE 243, 124 (1980).

[12] L.G. Shirley, "Speckle Decorrelation Techniques for Remote Sensing of Rough Objects," in OSA Annual Mtg. Tech. Dig. 18 (Optical Society of America, Washington, 1989), p. 208.

[13] L.G. Shirley, "Speckle Decorrelation," Proc. IRIS Targets, Backgrounds, and Discrimination 1, 123 (1990).

[14] D.J. Schertler and N. George, "Comparison of Wavelength Scanning and Pulse Echo Systems in Remote Sensing," Opt. Commun. 77, 91 (1990).

[15] L.G. Shirley, "Remote Sensing of Object Shape Using a Wavelength Scanning Laser Radar," in OSA Annual Mtg. Tech. Dig. 17 (Optical Society of America, Washington, 1991), p. 154.

[16] L.G. Shirley and J.R. Vivilecchia, "Target Characterization Using a Wavelength Scanning Laser Radar," Proc. Second Annual Automatic Target Recognizer System and Technology Conf. (1992).

[17] J.C. Marron and K.S. Schroeder, "Three-Dimensional Lensless Imaging Using Laser Frequency Diversity," Appl. Opt. 31, 255 (1992).

[18] J.C. Marron and T.J. Schulz, "Three-Dimensional, Fine-Resolution Imaging Using Laser Frequency Diversity," Opt. Lett. 17, 285 (1992).

[19] J.C. Marron, "Wavelength Decorrelation of Laser Speckle from Three-Dimensional Diffuse Objects," Opt. Commun. 88, 305 (1992).

[20] J.C. Dainty, ed., *Laser Speckle and Related Phenomena* (Springer-Verlag, Berlin, 1984).